applied sciences

MDPI

Article

Compressive Behavior of Oil Shale with Calcareous Concretion: Parametric Study

Jinxing Lyu [1,2], Jisen Shu [1], Liu Han [1,*], Gerson S. V. Tovele [1] and Tao Chen [1]

[1] School of Mines, China University of Mining and Technology, Xuzhou 221116, China; DB19020012B0YJ@cumt.edu.cn (J.L.); jsshu888@139.com (J.S.); fb19020001@cumt.edu.cn (G.S.V.T.); chentao2020@cumt.edu.cn (T.C.)

[2] School of Geology and Mining Engineering, Xinjiang University, Urumqi 830046, China

* Correspondence: hanliucumt@163.com; Tel.: +86-15862113698

Abstract: The non-uniformly distributed calcareous concretion among the oil shale in the Junggar basin of China has led to the difficulty in achieving the slope stability. This paper presents the numerical simulation of the behavior of oil shale with calcareous concretion via the Particle Flow Code (PFC2D) program based on the trial experimental test results. The critical parameters investigated in this research covered the size, distribution, strength, and number of the calcareous concretion. The following conclusions can be drawn based on the discussions and analysis: (1) the hard concretion always results in the high compressive strength of the specimen compared with that without concretion; (2) when the radius of the concretion size raised from 2.5 mm to 20 mm, the peak strength of tested specimens is approximately 50 MPa, whereas, the specimen with large concretion is much more ductile under compression; (3) the compressive behavior of tested specimens is similar even when the position of the concretion is variable; and (4) different from the specimens with only one concretion, these specimens contained two concretions featured with the double "X" failure mode. Meanwhile, the peak strength of the specimens with two hard concretions is about 2.5 times that of its counterparts with two soft concretions. The numerical simulation results are meaningful in guiding the design and analysis of the oil shale slope with the concretion.

Keywords: oil shale; calcareous concretion; compressive behavior; PFC2D; numerical simulation

Citation: Lyu, J.; Shu, J.; Han, L.; Tovele, G.S.V.; Chen, T. Compressive Behavior of Oil Shale with Calcareous Concretion: Parametric Study. *Appl. Sci.* **2021**, *11*, 11244. https://doi.org/10.3390/app112311244

Academic Editors: Mikhail O. Eremin and Pavel V. Makarov

Received: 20 October 2021
Accepted: 23 November 2021
Published: 26 November 2021

1. Introduction

As one of the largest deposited unconventional shales around the world, oil shale drew much attention either from the government or the industry in the past several decades [1–4]. How to excavate vast deposited oil shale effectively and cost-effectively is believed to be the huge challenge for most countries [5]. Different from these methods currently adopted by operators [6,7], it has been demonstrated that open-pit mining is the first choice for these zones with shallow depth. A good example is that in China, where more than 700 billion tons of oil shale were explored [8,9]. Among them, there are over 120 billion tons of oil shale distributed in the Junggar Basin, northwestern China, for which the mining depth is about 200 m [10].

If the open-pit mining method is adopted, as well noted, the slope stability is generally the most critical concern for industrial operators. The properties of the rock mass either in terms of the physical aspect or the mechanical response will be thus taken into consideration, which is initially obtained from the design aspect [10,11]. As previously stated by many scholars [12–14], these mechanical properties to be accounted for include the compressive and tensile strength of the rock mass, water content, as well as the weathering factors. In addition, both the specific component and micro-structures of the rock mass will influence the response of the rock mass under different loading conditions. As depicted in Figure 1, the existence of the concretions in the rock mass, in particular in the sedimentary

shale rock, will generally results in the unique mechanical behavior [15,16]. As a typical sedimentary shale rock, there are also many concretions observed in the Junggar Basin.

Figure 1. Carbonate concretions of the Rhinestreet shale [17].

These randomly distributed concretions (see Figure 1) will lead to the side effect on the stability of slope, when the rock mass is extracted via open-pit mining. In order to investigate the behavior of rock mass containing the concretions, much experimental and theoretical research was previously conducted. As documented in several literature reviews [18–20], it is not easy to obtain the natural rock samples containing the same concretion from the laboratory, and thus the result of which is not always reasonable. To fill the research gap and make sure the experimental tests are repeatable, the rock-like material was developed to get the identical specimens containing concretions as designed [9].

Even though the use of rock-like material provided the effective method to obtain the homogeneity specimens, the minor cracks or fractures initially distributed in the rock mass are usually neglected. To change the current situation with the use of rock-like material in the reproduction of the rock mass with concretions further, Zhu, Li et al. proposed the new experimental design program [20]. In their research, the specimens were drilled from the single rock mass firstly, and then the holes were cut from the prepared rock sample. After that, the fresh mixture was grouted into these holes to fabricate the rock specimen with concretions.

With the wide use of the large storage computing machine, the numerical simulation is accepted by more and more researchers, Numerical modelling is regarded as the other alternative option to understand the behavior of the rock mass with concretion better [21]. Among them, the particle flow code (PFC) program is believed to be one of the most powerful programs for mining engineering, in which the research objective is made of grain particles and is naturally heterogeneous [22,23]. It was well used in simulating the specimens made of different materials, such as the mixture of soil and rock [24] and the representative rock samples with the single crack [25].

Currently, there is no direct-related research, either in terms of the experimental tests or the numerical simulation, was conducted to explore the influence of concretions on the behavior of oil shale, although the existence of concretions in oil shale has drawn much attention, in particularly, for mining operators. Theoretically speaking, these non-uniformly distributed concretions will affect the stability of the oil shale slope, if the oil shale resource is excavated by via the open-pit mining method. Unfortunately, no evidence is available to support the mentioned conclusion. As a result, the stability control of the oil shale slope with concretions is correspondingly difficult.

Against this background, this paper presents the first-ever research on the uniaxial compressive behavior of the oil shale sample containing the concretion via the PFC2D program. This paper starts with the laboratory tests on the typical oil shale specimens with concretion to obtain the basic data, followed by the validation of the PFC model together with the determination of microscope parameters. Then, the systematic parametric study, covering the size, distribution, strength, and number of the concretion, was conducted. The main conclusions obtained from this research will be benefit to researchers in obtaining the

compressive behavior of oil shale containing concretions and provide the reference for the cost-effective excavation and control the stability of oil shale slope.

2. Laboratory Test

The laboratory tests were carried out aiming at exploring the difference between oil shale samples with or without the concretion. Several attempts previously failed to obtain the cylindrical specimens due to the non-uniformly distributed concretions in the rock mass. All cubic specimens are with a constant dimension of 50 × 50 × 50 mm, These specimens were prepared in accordance with the standard recommended by the International Society for Rock Mechanics (ISRM) [26]. Three cubic specimens were tested on the hydraulic 500 kN compression machine. The machine is controlled with a displacement controlling mode. The displacement speed is constantly set up of 1 mm/min, during which the axial load is applied on the top end of the surface until the crush of the specimen. As can be found from Figure 2, the selected specimen after the test is failed with the separation of the oil shale mass and calcareous concretion is obvious. The cracks generally occurred along the interface between the concretion and rock mass. In addition, some failures were found in the concretion itself.

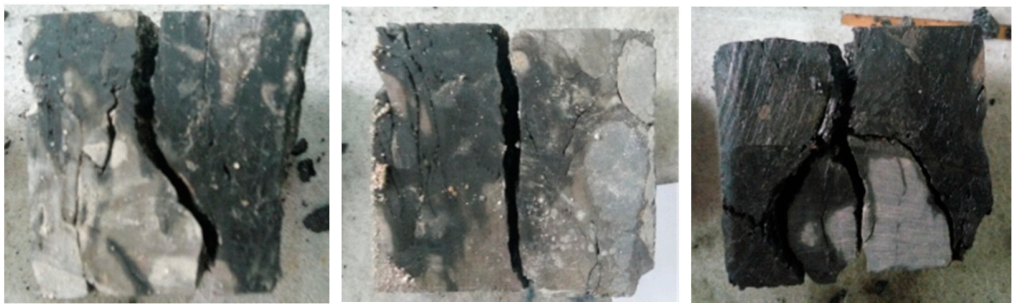

Figure 2. Typical failure modes of oil shale specimen (50 × 50 × 50 mm) containing the concretions after test.

Figure 3 depicts the compressive response of three tested specimens, in which the stress was calculated on the cross section of the cubic specimens. Whereas, the axial strain was manually calculated by the reading of the axial deformation. It is apparent that both the axial stress and axial strain of these three specimens are much different, although these specimens were drilled from the same rock mass. It indicated that the non-uniformly distributed concretions will significantly affect the compressive behavior of the oil shale.

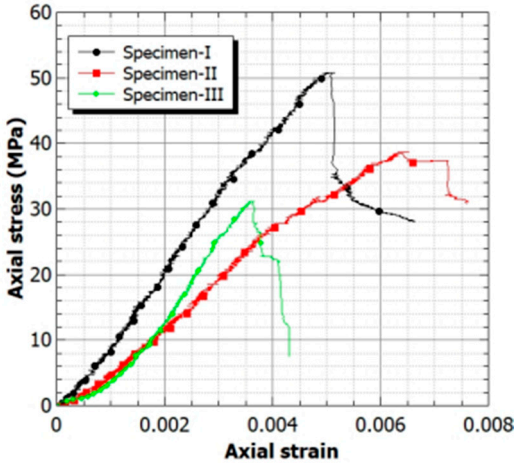

Figure 3. Relationship between axial stress and axial strain curves of tested specimens.

Because that the distribution of the concretion in oil shale is not always uniform, the design of the slope and the proposal of technical methods in controlling the stability of the rock mass are unreasonable, if they are all based on the mechanical behavior of the experimental test results.

3. Numerical Simulation of Oil Shale with Concretions

In the present research, the particle flow code (PFC) 2D (Version 5.0), provided by the Itasca Consulting Group, Inc. (Minneapolis, MN, USA) was adopted. To obtain the in-depth understating of the compressive behavior of oil shale with concretion, the systematic parametric study was conducted. The test variables in this research include the size, distribution, strength, and number of concretions in the rock mass, which were not easy to be investigated experimentally.

3.1. Numerical Set-Up of Oil Shale with Concretions

To make sure the constant of the numerical modelling and experimental tests, the base numerical model presented herein is in a square with the dimension of 50 mm. The base model was generated by the default procedure in PFC 2D (see Figure 4a,b).There are about 46,254 particles generated in rebuild the specimen within the closed square box made of rigid walls (i.e., top, bottom, and two sides). The maximum and minimum particle sizes of the balls are $5 \times e^{-3}$ and $7.5 \times e^{-3}$ with the given porosity of 0.008.

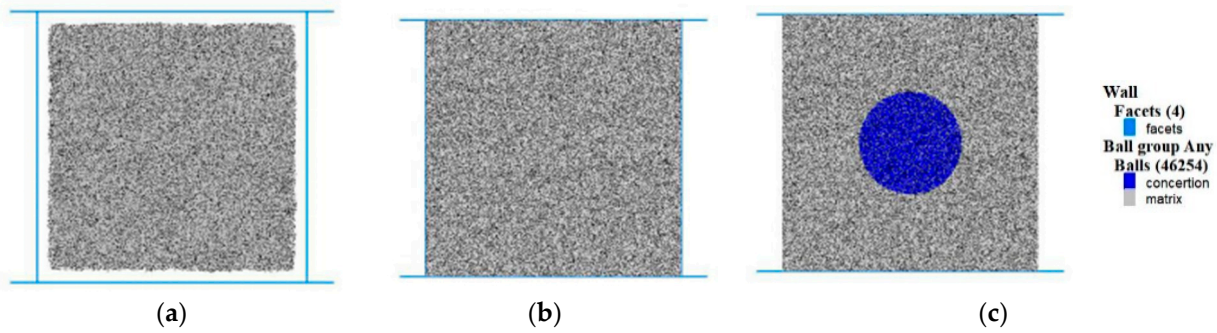

Figure 4. Flow chart for the establishment of the specimens: (**a**) generation of rock mass (matrix); (**b**) balancing the model; (**c**) determining and generating the concretion.

Once the base model of the rock mass (matrix) was established, the following steps were then applied to generate the inner concretion: (1) determining the position of the concretion, using the symmetrical point for reference; (2) differentiating the concretion from the rock mass through the user-defined program; (3) assigning the group names to the rock mass and concretion; and (4) giving the microscopic properties to the rock mass and the concretion, respectively.

Note that the side walls in the model will be removed when the numerical model with the concretion was established. Once the assignment of the microscopic parameters has been finished, the axial load can be applied to the rig walls in both sides of the established numerical model. The reproduced model can be then use to simulate the uniaxial compression test, which is similar to the tests carried out in the laboratory.

3.2. Tested Specimens

A total of 21 PFC2D models were established to investigate the effect of concretion on the behavior of oil shale. These PFC models were divided into five groups as shown in Figure 5, including one reference specimen without any concretion in Group 1 and 20 specimens covering the variable parameters in other groups.

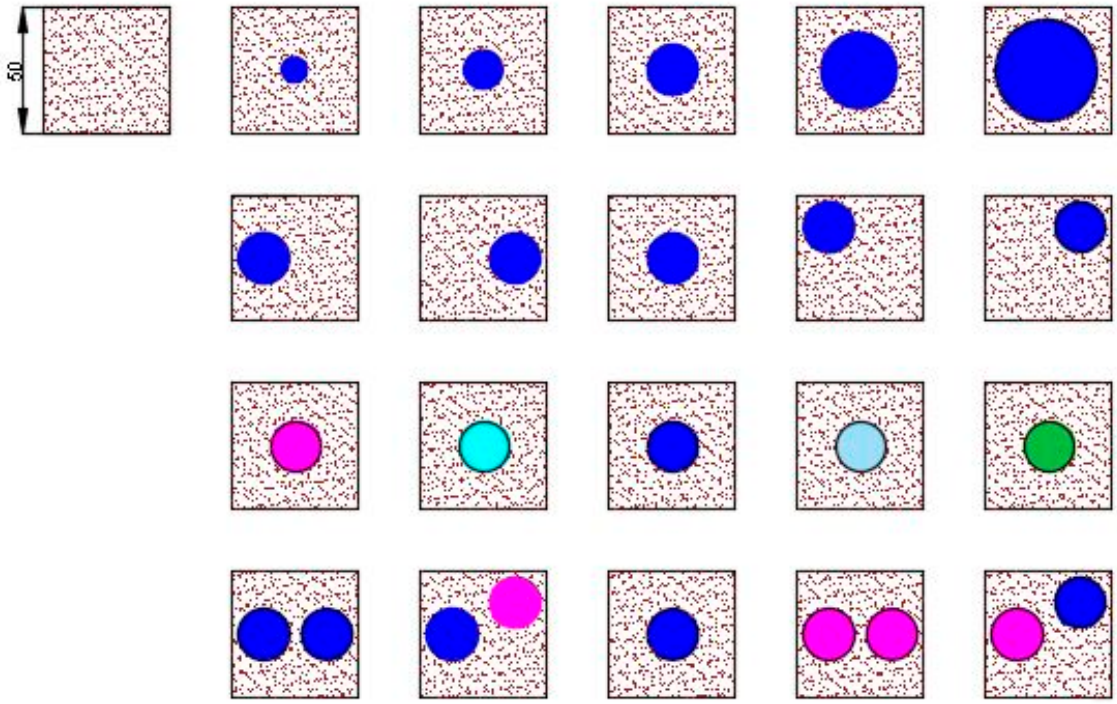

Figure 5. Test matrix.

In Group 2, rthere are five specimens were prepared, which can be used to explore the influence of concretion size. The only difference between these specimens is the size of the concretion, which ranges from 2.5 mm to 20 mm. These PFC models in Group 3 are different from each other in terms of the location of the concretion with a constant radius of 10 mm. These concretions are distributed apart from the center line for specimens G31 and G32 with the distance of 10 mm, while the other concretions are placed at the top corner of the specimens. In Group 4, the 10-mm-radius concretion was placed in the middle of the specimens, but the compressive strength was variable. The strength of these concretions is either lower or higher than that of the rock mass, which was used to investigate the effect of the compressive strength of the concretion. Note that five PFC models in Group 5 all have two concretions except for the reference specimen. The radius of the concretions is 10 mm, and these two concretions were uniformly placed at the middle of the specimens. It should be noted here that a different compressive strength was given to these concretions, which will help to explore the influence of the number and strength of the concretion.

3.3. Selection of Bond Model

In the PFC 2D program, there are many build-in models designed for different purposes [27–29]. Among them, the widely used model for geomechanics and mining engineering is the linear parallel-bonded model (also called the Pb model). In this research, the linear model was adopted to simulate the interactions between the particles and the rigid wall, while the Pb model was used to simulate the connections of the particles either for the rock mass of oil shale or the inner concretion.

Figure 6a shows the illustration of the linear model, in which there is no contact moment in the linear model. The linear model only transfers the force. The contact force is the combination of the linear and dashpot components. Herein, the linear element usually provides the linear elastic, frictional behavior by the linear spring with a constant normal and shear stiffness. Whereas, the dashpot force is produced through the dashpots. It is therefore regarded as the ideal model to simulate the intersection between the rock mass and the loading platen.

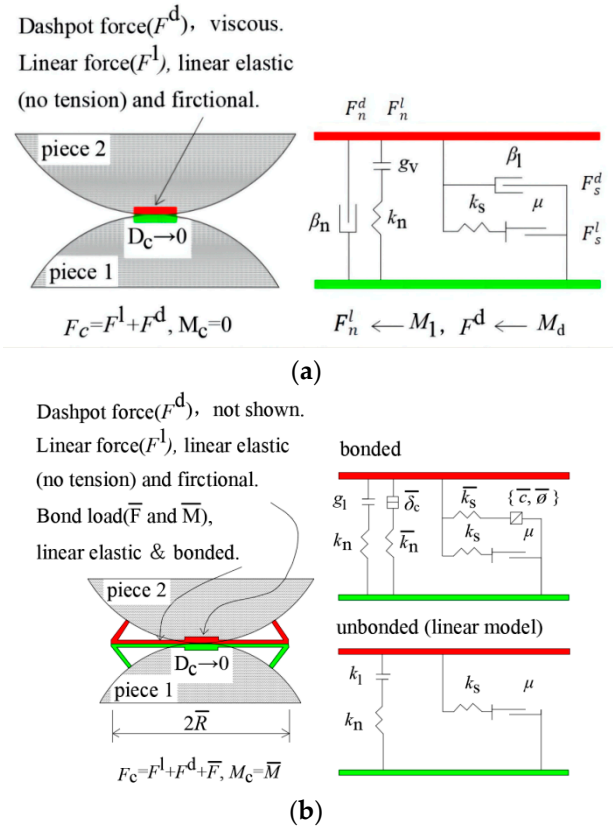

Figure 6. Illustration of the model used in this research [27]. (**a**) the illustration of the linear model; (**b**) the connection between two different particles is controlled by the linear parallel bond model.

As seen from Figure 6b, the connection between two different particles is controlled by the linear parallel bond model, which belongs to the type of linear based model as well. Different from the linear model descripted above, the linear parallel bond model increases additional interface between the rigid balls. The new feature of the bonded interface is that it can resist the rotation until the failure of the bond. Once these connections are broken, the second interface will not carry load. Then, the linear parallel model becomes the linear model. Considering the real failure mode and mechanical behavior of the rock mass, it is feasible to use the liner parallel model to simulate the oil shale with concretions.

In the Pb model, both the force and moment are transmitted by the parallel bond. The Mohr–Coulomb criterion is adopted to simulate the discs in PFC2D. As stated earlier, the Pb model is updated on the linear model, and thus the force-displacement law including the contact force (F_c) and contact moment (M_c) can be expressed below [27]:

$$F_c = F^l + F^d + \overline{F}, M_c = \overline{M} \tag{1}$$

in which F^l, F^d, F are the linear force, dashpot force, and the bond force, respectively.

Note that the values of both F^l and F^d are equal to their counterparts in the linear model. Herein, the force in the Pb model is made of the normal force ($\overline{F}_n$) and shear force ($\overline{F}_s$), whereas the moment in the Pb model is resolved into a twisting and bending moment, as shown in Equations (2) and (3):

$$\overline{F} = -\overline{F}_n \hat{n}_c + \overline{F}_s \tag{2}$$

$$\overline{M} = -\overline{M}_t \hat{n}_c + \overline{M}_b \left(\text{2D model}: \ \overline{M}_t \equiv 0\right) \tag{3}$$

As indicated in Equations (4) and (5), the shear force and bending moment can be expressed below:

$$\overline{F}_s = \overline{F}_{ss} \hat{s}_c + \overline{F}_{st} \hat{t}_c \left(\text{2D model}: \ \overline{F}_{ss} \equiv 0\right) \tag{4}$$

$$\overline{M}_b = \overline{M}_{bs}\hat{s}_c + \overline{M}_{bt}\hat{t}_c \left(\text{2D model}: \ \overline{M}_{bt} \equiv 0\right) \quad (5)$$

3.4. Determination of Micromechanical Parameters

There is a big difference between the conventional finite element modeling and DEM modelling, the required in-put parameters of the former can be easily obtained from the experimental tests, it is impossible to get the micro-mechanics properties requested by the PFC model. Therefore, the trial-error method is generally adopted to reproduce the macro-mechanical behavior of the tested specimen [30–34].

Considering the limitation of the experimental data about the compressive behavior of the integrity oil shale, in this research, the averaged compressive strength of these three specimens presented in Figure 3 (i.e., 40 MPa) was adopted herein to get the micromechanical parameters for the base model. It should be noted that herein the properties of the linear model were adopted from other research, considering that the intersection between the rock mass and loading platen will not significantly affect the simulation results if all parameters used for each model are constant.

By adopting the trail-error method, the microscopic parameters of the parallel-bonded model are presented in Table 1, All these parameters are all calibrated on the bases of the base model (i.e., 44 MPa and 0.005), because both the model size and the particle size will affect the simulation.

Table 1. Microscopic parameters of the linear model.

Properties	Rock Mass	Concretion	Concretion *
Effective modulus, emod (GPa)	3.8	3.8	$3.8 \times \gamma$
Bond effective modulus, pb_emod (GPa)	3.8	3.8	$3.8 \times \gamma$
Tensile strength, pb_ten (MPa)	1.0	5.0	$1.0 \times \gamma$
Cohesion strength, pb_coh (MPa)	1.5	7.5	$1.5 \times \gamma$
Reference gap	$0.75e^{-4}$	$0.75e^{-4}$	$0.75e^{-4}$
Friction angle (°)	35	35	35
Friction coefficient	0.577	0.577	0.577

It is not easy to get the compressive behavior of the concretion in the rock mass. Therefore, in this research, the variable concretions with different mechanical properties were obtained by changing the microscopic parameters through changing the value of these microscopic parameters shown in Table 1. To achieve this aim, the values of γ in this research are 0.25, 0.5, 1.25, and 1.5, respectively.

4. Results and Discussions

In this section, the effect of the critical parameters, including the size, distribution, strength, and number of the concretions on the response of the oil shale under compression loading are discussed based on the numerical simulation results.

4.1. Effect of the Size of Concretion

The typical failure mode of the specimens with different concretion sizes are presented in Figure 7a. It is obvious in Figure 7 that all specimens with concretion are failed with the separation of the rock mass and the concretion along the interface in between, which agrees well with the experimental observation presented earlier. No obvious damages can be seen from the surface of the concretion itself, indicating that the concretion size will not significantly affect the failure mode when other parameters are the same. However, with the increase in the concretion size, the affected zone with micro fractures was enlarged, which can be found from Figure 7b. It is not difficult to explain because the integrity of the specimen is relevant to the size of the concretion.

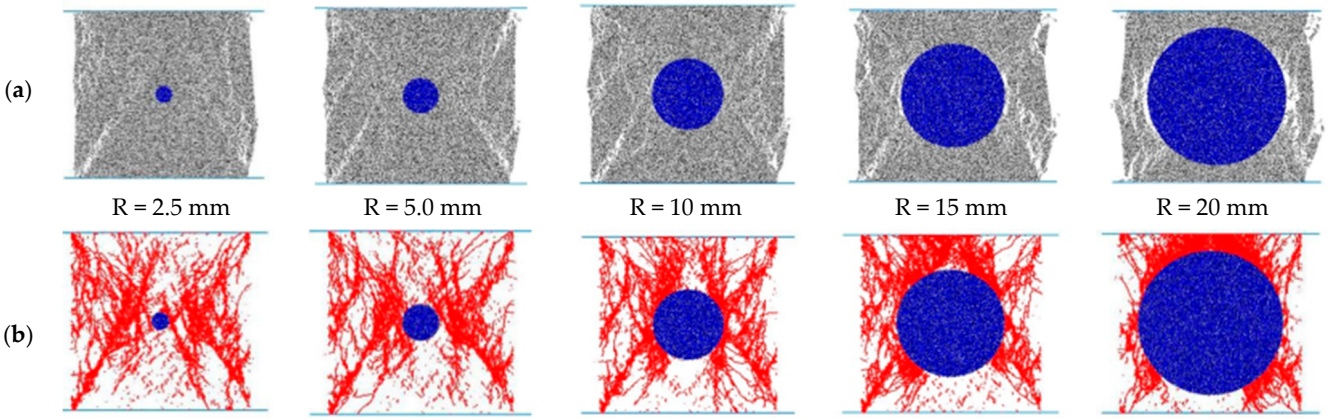

Figure 7. Typical failure modes of specimens in Group 2: (**a**) failure mode of specimen; (**b**) failure mode of concretion.

Although the concretion size will not affect the failure mode of the specimen, it is much different when the axial stress and axial strain curves of these specimens with various concretion sizes are compared, as shown in Figure 8. Compared with the base model (reference specimen) without the concretion, the existence of the concretion results in the enhancement of the overall compressive strength of specimens. This is mainly attributed to the higher strength of the concretion.

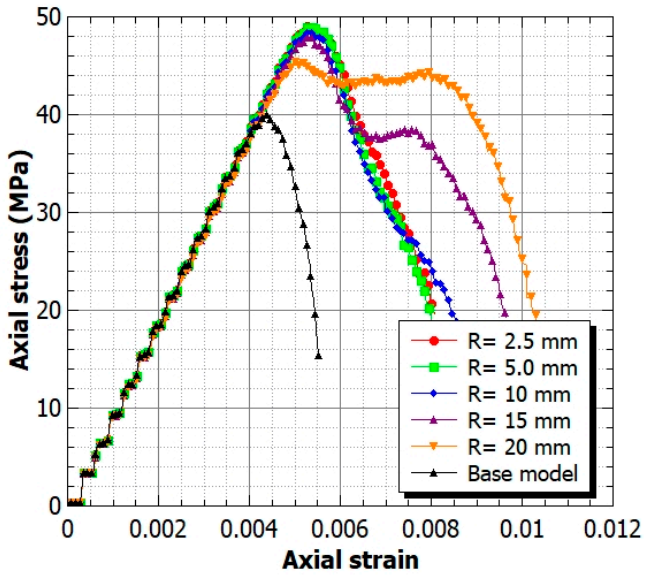

Figure 8. Axial stress, axial strain curves of tested specimens in Group 2.

It can also be found from Figure 8 that the peak stress of these specimens with concretion is similar, although the post-peak behavior is not always constant as depicted in Figure 8. That is, the ductility of these specimens with large concretion seems to be superior to some extent.

4.2. Effect of the Position of Concretion

As depicted in Figure 9, all specimens with the hard concretion distributed at different locations of the rock mass share the similar failure mode. All these specimens are featured with the splitting of the rock mass and concretion along the interface in between. When the fractures are presented together with the concretion, it is apparent that there is no crack that occurred around the concretion. If the concretion is placed in the middle of the specimen, the failure mode looks to be an "X" shape, which is the typical characteristics of the shear failure. If the concretion is placed apart from the center line but still in the

mid height of the specimen, the "X" shape failure will not be obvious. Instead, the center point will move forward to the center of the concretion associated with the crush observed around the edge of the square specimens. The same observation can be also found from the specimens contained in the concretion around the corner of the specimens.

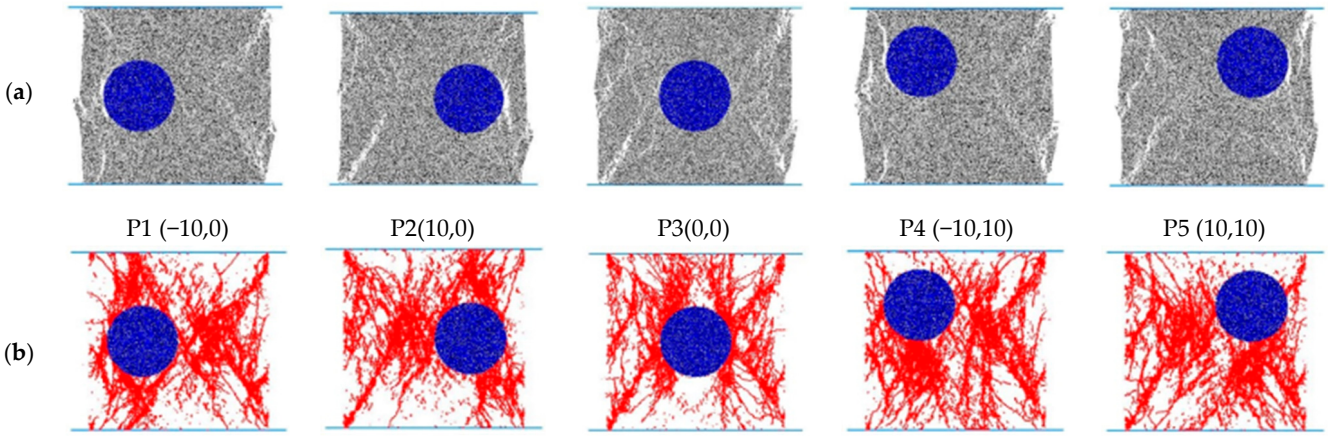

Figure 9. Typical failure modes of specimens in Group 3: (**a**) failure mode of specimen; (**b**) failure mode of concretion.

The other notable observation shown in Figure 10 is that the difference between these specimens with variable distributions of the concretion is neglected, either in terms of the compressive strength or the ductility corresponding to the peak strength. This is mainly attributed to the fact that all contacts between the rock mass and concretion are all the same. As a result, the specific distribution of the concretion will not affect the compressive behavior of the specimen, although the failure modes are somewhat different.

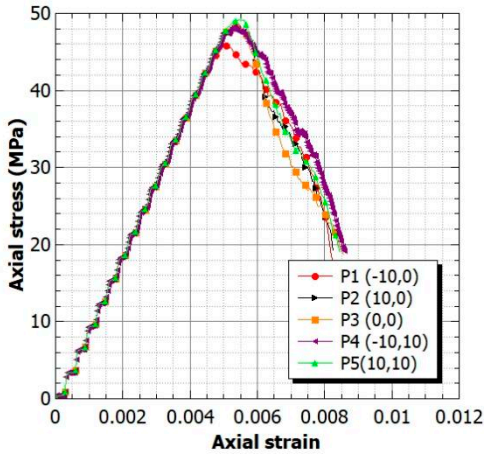

Figure 10. Axial stress, axial strain curves of tested specimens in Group 3.

4.3. Effect of the Concretion Strength

As discussed above, the representative failure mode of the specimen is the separation of the rock mass and included concretion, when the compressive strength of the concretion is higher than that of the rock mass. In this section, the softer concretions were placed in the middle of the specimens to explore the effects of the concretion strength.

It is apparent in Figure 11 that all specimens with the softer concretion are failed with the crack of the concretion itself, which is much different from the reference specimen with hard concretion. It can be also obtained from Figure 11 that the number of cracks inside the concretion decreases with the concretion strength. Correspondingly, the shear failure with the "X" shape becomes not obvious, indicating that the ductility of the specimen may be enhanced.

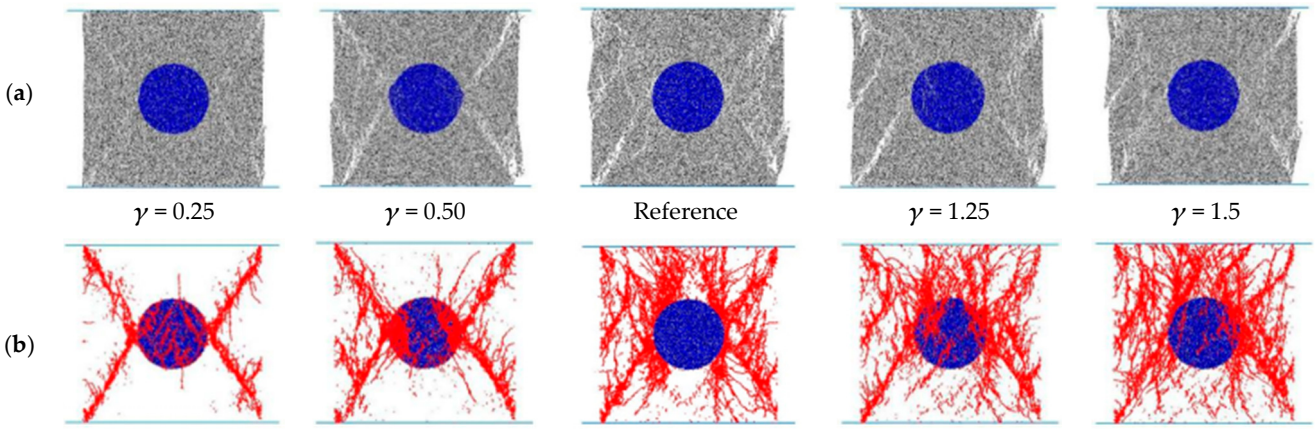

Figure 11. Typical failure modes of specimens in Group 4: (**a**) failure mode of specimen; (**b**) failure mode of concretion.

When the axial stress, axial strain curves of specimens from Group 4 are plotted in Figure 12 together with the reference specimen, it can be found out that both the compressive strength and the ductility of the specimens increase with the concretion strength. The higher strength of the concretion always results in the higher compressive strength of the specimens. However, the above conclusion is only suitable for specimens in the cases for which the concretion strength is somehow lower than that of the rock mass.

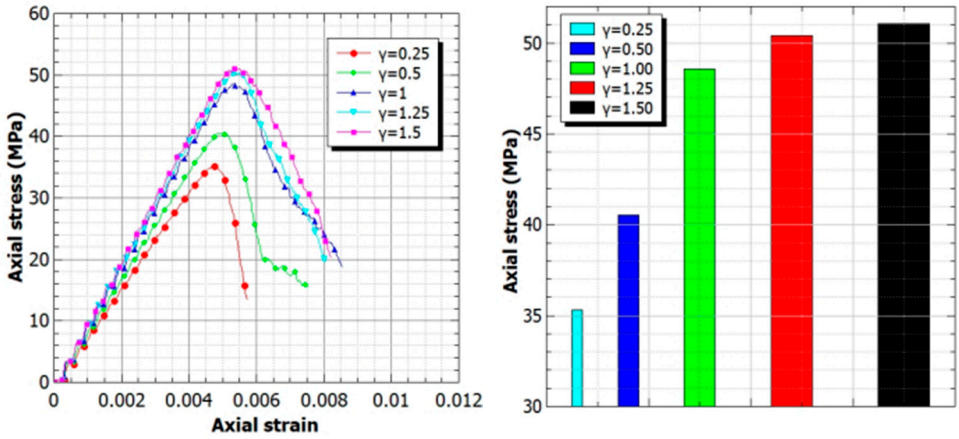

Figure 12. Axial stress, axial strain curves of tested specimens in Group 4.

4.4. Effect of the Number of Concretions

Different from these specimens with only one concretion, as shown in Figure 13, these specimens from Group 5 show the unique failure modes. As discussed earlier, the typical shear failure with the "X" shape crack is generally obtained for specimens with the sole concretion. When there are two concretions distributed in the rock mass, the double "X" failure mode can be seen from Figure 13. When the cracks of the specimens are presented respectively, it can be found that: (1) two concretions were all crushed, and the double shear failure modes seem to be more obvious for these soft concretions; (2) the shear cracks always occurred around the hard concretions without obvious cracks in the concretions; (3) the soft concretion will be crushed, but the hard one will maintain integrity associated with the separation of the rock mass and the hard concretion.

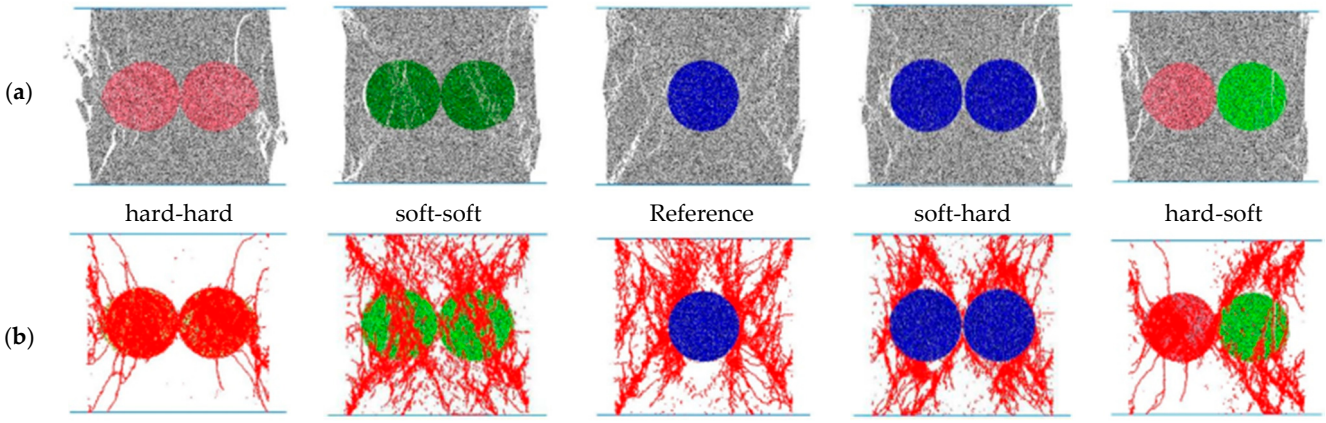

Figure 13. Typical failure modes of specimens in Group 5: (**a**) failure mode of specimen; (**b**) failure mode of concretion.

Figure 14 compares the axial stress, axial strain curves of specimens containing two concretions, in which the compressive strength of the concretions is much different. As expected, the compressive strength of the specimens with two soft concretions is the lowest, followed by the specimens with one hard concretion and one soft one. The specimen with two hard concretions has the highest compressive strength.

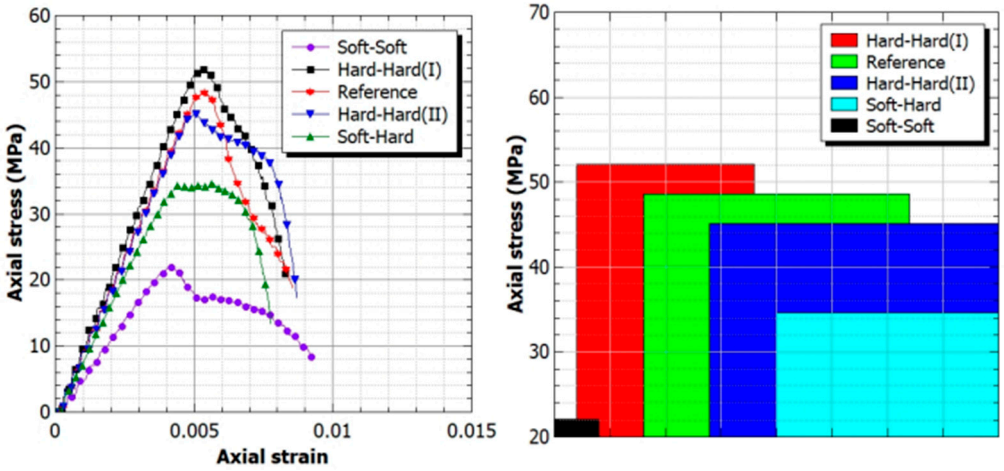

Figure 14. Axial stress, axial strain curves of tested specimens in Group 5.

The above discussions agree well with the conclusion obtained from Section 4.3 for the specimens with one concretion, suggesting that the existence of the hard concretion will enhance the overall compressive strength of the specimen.

5. Conclusions

This paper has presented a systematic numerical simulation on the compressive behavior of oil shale with the concretion. The Particle Flow Code (PFC2D) program was adopted. The laboratory tests were firstly conducted and based on the base model that was established. A large range of variable parameters, including the size, distribution, strength, and number of the concretions, was well investigated through the parametric study. According to the numerical simulation results and discussions, the following conclusions can be drawn:

(1) For the specimens with a hard concretion, the typical failure mode is with the shear cracks, which were featured with the separation of the rock mass and concretion along the interface;

(2) The failure mode and the compressive strength of these specimens with a hard concretion will not be significantly affected by the concretion size. However, the post peak behavior of specimens will be somewhat related to the concretion size;
(3) The axial strain and axial stress curves of specimens are not sensitive to the distribution of the concretion, although the failure mode will be a little different;
(4) When the number of the concretion increases from one to two, both the failure mode and compressive behavior of the specimens were significantly affected.

Although the main aim of this first-ever research is to explore the the compressive behavior of oil shale with the concertation, in fact, only some typical parameters are accounted for currently. In the coming future, the effects of the composition of the shale, the proportion of organic carbon, the composition of the hydrocarbon component, and the porosity of the shale should also be well investigated. Note that the concretions are extremely uneven in crystal size, and the lower part has a fine-grained structure, and the upper part is represented by giant-grained crystals, and thus the influence of structural characteristics should also be accounted for in future research.

Author Contributions: Conceptualization, J.L. and L.H.; methodology, J.S.; software, L.H.; validation, T.C.; formal analysis, J.L. and G.S.V.T.; investigation, T.C.; resources, L.H.; data curation, T.C.; writing—original draft preparation, J.L.; writing—review and editing, G.S.V.T.; visualization, J.L.; supervision, J.S.; project administration, J.L.; funding acquisition, L.H. All authors have read and agreed to the published version of the manuscript.

Funding: The authors are grateful for the financial support by the National Natural Science Foundation of China (51804298 and 51774271).

Institutional Review Board Statement: Not applicable.

Informed Consent Statement: Not applicable.

Data Availability Statement: Not applicable.

Acknowledgments: The authors would like to express thanks to the National Natural Science Foundation of China for their financial support. We are also grateful to the academic editor and three anonymous reviewers for providing constructive suggestions.

Conflicts of Interest: There are no conflict of interest in this paper.

References

1. Soone, J.; Doilov, S. Sustainable utilization of oil shale resources and comparison of contemporary technologies used for oil shale processing. *Oil Shale* **2003**, *20*, 311–323.
2. Dyni, J.R. *Geology and Resources of Some World Oil-Shale Deposits, Scientific Investigations Report 2005–5294*; U.S. Geological Survey: Reston, VA, USA, 2006; p. 42.
3. Torres, M.; Portugau, P.; Castiglioni, J.; Cuña, A.; Yermán, L. Co-combustion behaviours of a low calorific Uruguayan Oil Shale with biomass wastes. *Fuel* **2020**, *266*, 117118. [CrossRef]
4. Jia, B.; Chen, Z.; Xian, C. Investigations of CO_2 storage capacity and flow behavior in shale formation. *J. Pet. Sci. Eng.* **2021**, *208*, 109659. [CrossRef]
5. Allix, P.; Burnham, A.; Fowler, T.; Herron, M.; Kleinberg, R.; Symington, B. Coaxing oil from shale. *Oilfield Rev.* **2010**, *22*, 4–15.
6. Thorne, H.M.; Stanfield, K.E.; Dinneen, G.; Murphy, W. *Oil-Shale Technology: A Review*; US Department of the Interior, Bureau of Mines: Washington, WA, USA, 1964.
7. Han, X.; Kulaots, I.; Jiang, X.; Suuberg, E.M. Review of oil shale semicoke and its combustion utilization. *Fuel* **2014**, *126*, 143–161. [CrossRef]
8. Qian, J.; Wang, J.; Li, S. Oil shale development in China. *Oil Shale* **2003**, *20*, 356–359.
9. Cao, Y.; Shen, W.; Burlion, N.; Shao, J.-F. Effects of inclusions and pores on plastic and visco plastic deformation of rock-like materials. *Int. J. Plast.* **2018**, *108*, 107–124. [CrossRef]
10. Zhao, H.-C.; Zhang, X.-L.; Han, G.; Chen, H. Experimental investigation on the physical and mechanical properties deterioration of oil shale subjected to freeze-thaw cycles. *Arab. J. Geosci.* **2019**, *12*, 531. [CrossRef]
11. Oh, S.; Lu, N. Slope stability analysis under unsaturated conditions: Case studies of rainfall-induced failure of cut slopes. *Eng. Geol.* **2015**, *184*, 96–103. [CrossRef]

12. Wang, X.; Zhang, P.; Li, J.; Wang, N. Study on steep slope stability of coal mine under open-pit and underground mining. In Proceedings of the 2011 International Conference on Materials for Renewable Energy & Environment, Shanghai, China, 20–22 May 2011.
13. Cho, Y.-C.; Song, Y.-S. Deformation measurements and a stability analysis of the slope at a coal mine waste dump. *Ecol. Eng.* **2014**, *68*, 189–199. [CrossRef]
14. Vinoth, S.; Kumar, L.A. Applying real time seismic monitoring technology for slope stability assessment—An Indian opencast coal mine perspective. *Int. J. Min. Sci. Technol.* **2014**, *24*, 75–80. [CrossRef]
15. Valgma, I.; Reinsalu, E.; Sabanov, S.; Karu, V. Quality control of oil shale production in Estonian mines. *Oil Shale* **2010**, *27*, 239. [CrossRef]
16. Wolela, A. Sedimentation, organic maturity, and petroleum potential of the Oligocene–Miocene oil shale deposits, Yayu Basin, southwestern Ethiopia. *AAPG Bull.* **2010**, *94*, 643–663. [CrossRef]
17. Lash, G.G.; Blood, D.R. The Upper Devonian Rhinestreet Black Shale of Western New York State—Evolution of a Hydrocarbon System. In *New York State Geological Association, 78th Annual Meeting Guidebook*; University at Buffalo: Buffalo, NY, USA, 2006.
18. Wu, Z.; Wong, L.N.Y. Modeling cracking behavior of rock mass containing inclusions using the enriched numerical manifold method. *Eng. Geol.* **2013**, *162*, 1–13. [CrossRef]
19. Li, M.; Liang, L.; Fan, Y. Characteristics of Hydraulic Fracture in Heterogeneous Rock with Distributed Hard Inclusions. In *Proceedings of GeoShanghai 2018 International Conference*; Springer: Singapore, 2018.
20. Zhu, Q.; Li, D.; Han, Z.; Li, X.; Zhou, Z. Mechanical properties and fracture evolution of sandstone specimens containing different inclusions under uniaxial compression. *Int. J. Rock Mech. Min. Sci.* **2019**, *115*, 33–47. [CrossRef]
21. Li, M.; Guo, P.; Stolle, D.; Liang, L. Modeling method for a rock matrix with inclusions distributed and hydraulic fracturing characteristics. *J. Pet. Sci. Eng.* **2017**, *157*, 409–421. [CrossRef]
22. Tan, L.; Ren, T.; Dou, L.; Yang, X.; Qiao, M.; Peng, H. Analytical stress solution and mechanical properties for rock mass containing a hole with complex shape. *Theor. Appl. Fract. Mech.* **2021**, *114*, 103002. [CrossRef]
23. Zhang, L.; Ren, T.; Li, X.; Tan, L. Acoustic emission, damage and cracking evolution of intact coal under compressive loads: Experimental and discrete element modelling. *Eng. Fract. Mech.* **2021**, *252*, 107690. [CrossRef]
24. Shan, P.; Lai, X. Mesoscopic structure PFC∼ 2D model of soil rock mixture based on digital image. *J. Vis. Commun. Image Represent.* **2019**, *58*, 407–415. [CrossRef]
25. Huang, D.; Cen, D.F.; Huang, R.Q. Influence of medium strain rate on sandstone with a single pre-crack under uniaxial compression using PFC simulation. *Rock Soil Mech.* **2013**, *34*, 535–545.
26. ISRM. Suggested Methods for Determining Uniaxial Compressive Strength and Deformability of Rock Materials, ISRM Committee on Standardization of Laboratory Tests. *Int. J. Rock Mech. Min. Sci.* **1979**, *16*, 137–140. [CrossRef]
27. Itasca, C. *PFC–Particle Flow Code, Ver. 5.0*; Itasca Consulting Group Minneapolis: Minneapolis, MN, USA, 2017.
28. Zhou, Z.; Tan, L.; Cai, X. Water Infusion on the Stability of Coal Specimen under Different Static Stress Conditions. *Appl. Sci.* **2020**, *10*, 2043. [CrossRef]
29. Tan, L.; Ren, T.; Dou, L.; Yang, X.; Cai, X.; Qiao, M. Analytical stress solution for rock mass containing two holes based on an improved Schwarz alternating method. *Theor. Appl. Fract. Mech.* **2021**, *116*, 103092. [CrossRef]
30. Haeri, H.; Sarfarazi, V. Numerical simulation of tensile failure of concrete using particle flow code (PFC). *Comput. Concr.* **2016**, *18*, 53–68. [CrossRef]
31. Wang, P.; Yang, T.; Yu, Q.; Liu, H.; Zhang, P. Characterization on jointed rock masses based on PFC2D. *Front. Struct. Civ. Eng.* **2013**, *7*, 32–38. [CrossRef]
32. Tan, L.; Ren, T.; Dou, L.; Cai, X.; Yang, X.; Zhou, Q. Dynamic response and fracture evolution of marble specimens containing rectangular cavities subjected to dynamic loading. *Bull. Eng. Geol. Environ.* **2021**, *80*, 7701–7716. [CrossRef]
33. Hadjigeorgiou, J.; Esmaieli, K.; Grenon, M. Stability analysis of vertical excavations in hard rock by integrating a fracture system into a PFC model. *Tunn. Undergr. Space Technol.* **2009**, *24*, 296–308. [CrossRef]
34. Potyondy, D.O. Parallel-bond refinements to match macroproperties of hard rock. *Contin. Distinct Elem. Numer. Modeling Geomech.* **2011**.